Virus Research 342 (2024) 199335

Contents lists available at ScienceDirect

Virus Research

journal homepage: www.elsevier.com/locate/virusres

Systems genetics of influenza A virus-infected mice identifies TRIM21 as a critical regulator of pulmonary innate immune response

Zhuoyuan Alex Li [a,1], Akhilesh Kumar Bajpai [a,1], Ruixue Wang [b], Yaxin Liu [b,c], Richard J. Webby [d], Esther Wilk [e], Weikuan Gu [c], Klaus Schughart [b,f], Kui Li [b,**], Lu Lu [a,*]

[a] Department of Genetics, Genomics and Informatics, University of Tennessee Health Science Center, Memphis, TN, USA
[b] Department of Microbiology, Immunology and Biochemistry, University of Tennessee Health Science Center, Memphis, TN, USA
[c] Department of Orthopaedic Surgery and Biomedical Engineering, University of Tennessee Health Science Center, Memphis, TN, USA
[d] Department of Infectious Diseases, St Jude Children's Research Hospital, Memphis, TN, USA
[e] Rochus Mummert Healthcare Consulting GmbH, Hannover, Germany
[f] Institute of Virology Münster, University of Münster, Münster, Germany

ARTICLE INFO

Keywords:
TRIM21
Influenza A virus
BXD mice
Transcriptome
Recombinant inbred
Innate immunity
Modeling

ABSTRACT

Tripartite motif 21 (TRIM21) is a cytosolic Fc receptor that targets antibody-bound, internalized pathogens for destruction. Apart from this intrinsic defense role, TRIM21 is implicated in autoimmune diseases, inflammation, and autophagy. Whether TRIM21 participates in host interactions with influenza A virus (IAV), however, is unknown. By computational modeling of body weight and lung transcriptome data from the BXD parents (C57BL/6 J (B6) and DBA/2 J (D2)) and 41 BXD mouse strains challenged by IAV, we reveal that a *Trim21*-associated gene network modulates the early host responses to IAV infection. *Trim21* transcripts were significantly upregulated in infected mice of both B6 and D2 backgrounds. Its expression was significantly higher in infected D2 than in infected B6 early after infection and significantly correlated with body weight loss. We identified significant trans-eQTL on chromosome 14 that regulates *Trim21* expression. *Nr1d2* and *Il3ra* were among the strongest candidate genes. Pathway analysis found *Trim21* to be involved in inflammation and immunity related pathways, such as inflammation signaling pathways (TNF, IL-17, and NF-κB), viral detection signaling pathways (NOD-like and RIG-I-like), influenza, and other respiratory viral infections. Knockdown of TRIM21 in human lung epithelial A549 cells significantly augmented IAV-induced expression of *IFNB1, IFNL1, CCL5, CXCL10*, and IFN-stimulated genes including *DDX58* and *IFIH1*, among others. Our data suggest that a TRIM21-associated gene network is involved in several aspects of inflammation and viral detection mechanisms during IAV infection. We identify and validate TRIM21 as a critical regulator of innate immune responses to IAV in human lung epithelial cells.

1. Introduction

Influenza A viruses (IAVs) cause seasonal epidemics and occasionally lead to outbreaks of pandemic potential, posing a major public health challenge associated with significant morbidity and mortality. Infections with IAVs in vivo elicit robust host responses in the respiratory tract, including the induction of interferon (IFN) family of antiviral cytokines and interferon-stimulated genes (ISGs) and production of proinflammatory mediators, which collectively limit viral replication and spread but can inflict deleterious tissue damage if uncontrolled. As such, the timing and magnitude, as well as a delicate balance of these early innate immune responses are believed to dictate influenza disease pathogenesis and infection outcome. A deeper understanding of the host genes and gene networks that operate in response to IAV infection is critically needed and could inform therapeutic and/or prophylactic countermeasures.

Classified within the tripartite motif protein (TRIM) family of E3 ubiquitin ligases, TRIM21 (also known as RO52) is an intracellular antibody receptor that is expressed in most human tissues (Mallery et al., 2010). By binding to the Fc domain of immunoglobulins, TRIM21

* Corresponding author at: Department of Genetics, Genomics and Informatics, University of Tennessee Health Science Center, TN 38163, USA.
** Corresponding author at: Department of Microbiology, Immunology and Biochemistry, University of Tennessee Health Science Center, TN 38163, USA.
E-mail addresses: kli1@uthsc.edu (K. Li), llu@uthsc.edu (L. Lu).
[1] Z.A.L. and A.K.B. contributed equally to this work.

https://doi.org/10.1016/j.virusres.2024.199335
Received 24 December 2023; Received in revised form 5 February 2024; Accepted 5 February 2024

targets antibody-bound pathogens that have gained access to the cytoplasm of host cells for degradation. In addition to its immune surveillance role, TRIM21 is implicated in several autoimmune disorders (Oke and Wahren-Herlenius, 2012) often associated with hyperactivated type 1 IFN response. For instance, TRIM21 autoantibodies are frequently detected in systemic lupus erythematosus and Sjögren's syndrome. The precise involvement of TRIM21 in these inflammatory disorders remains murky. Intriguingly, with itself being an ISG product, TRIM21 suppresses IFN response by targeting a pivotal transcription factor, IFN-regulatory factor-3 (IRF3) for degradation by acting as an autophagic receptor (Kimura et al., 2017). However, the effect on IRF3-dependent IFN signaling reported for TRIM21 has not been consistent and likely is cell type- and/or infection setting-dependent, with both positive and negative regulations having been reported (reviewed in (Jones et al., 2021)). Thus far, relatively little research has been conducted on TRIM21 regarding its potential role(s) in non-autoimmune diseases. Given the recent observations that TRIM21 participates in regulating autophagy (Kimura et al., 2015) including that induced by IAV infection (Sparrer et al., 2017), we hypothesized that TRIM21 and/or its associated gene networks may play a part in modulating pathogenesis of and/or host responses to IAV infection.

It is well known that human diseases are a result of complex interactions between genetic and environmental factors. As one of the best characterized genetic reference populations, the BXD recombinant inbred (RI) mice derived from crossing B6 and D2 inbred strains have been widely used to study genetic basis of disease phenotypes. With ~150 fully sequenced strains and ~6 million sequence variants, BXD RI mice are suited as a diversity platform to define genetic variations linked to various diseases, including microbial infections. Previously, we and others have successfully employed the BXD platform to explore genetic factors that influence influenza virus susceptibility (Xu et al., 2020; Boon et al., 2009; Nedelko et al., 2012), based on striking differences in viral replication and disease severity between parental B6 and D2 and across the BXD strains. In this study, we set out to investigate whether *Trim21*-associated gene networks are involved in modulating the innate immune response to IAV infection, by mining the lung transcriptomics and weight loss data accrued from a subset of BXDs challenged with IAV (H1N1). We segregated differences in *Trim21* expression between the B6 and D2 strains, then used systems genetics approach to model the *Trim21* upstream/downstream regulators, genetic networks, and genetic pathways, to lend insights into mechanisms of host responses to IAV infection. Finally, we selected TRIM21 for functional validation using RNAi approach in a human lung epithelial cell culture model of IAV infection. Our data suggest TRIM21 negatively regulates innate antiviral immune responses to IAV in ways that modulate disease pathogenesis.

2. Methods

2.1. Ethics statement

All experiments in mice were approved by an external committee according to the German national guidelines of the animal welfare law (for B6 and D2 parental experiments) and the UTHSC Institutional Animal Care and Use Committee (for BXD experiments), and the protocol in Germany has been reviewed and approved by an ethics committee as described in the regulations from the German Bundesministerium für Ernährung, Landwirtschaft und Verbraucherschutzand, and detailed in the "Tierschutzkommissions-Verordnung vom 23. Juni 1987 (BGBl. I S. 1557)" (http://www.gesetze-im-internet.de/ bundesrecht/tierschkomv/gesamt.pdf). Subsequently, the protocol has been formally approved by the 'Niedersächsisches Landesamt für Verbraucherschutz und Lebensmittelsicherheit, Oldenburg, Germany' (Permit Number: 3392 42,502–04–13/1234).

2.2. Infection of mice

We used female mice bred at the University of Tennessee Health Science Center (UTHSC) for BXD infections, and mice obtained from Janvier (France) for infection of BXD parental strains (B6 and D2 mice). Animals were housed at UTHSC or at the Helmholtz Centre for Infection Research (HZI) and maintained on a 12:12 light/dark cycle, with ad libitum access to food and water. Original stocks of mouse-adapted A/Puerto Rico/8/34 (H1N1, PR8M) virus were obtained from Stefan Ludwig, University of Münster. Virus stocks were propagated in the chorioallantoic cavity of 10-day-old pathogen-free embryonated chicken eggs for 48 h at 37 °C. Viral titer was determined using a focus-forming unit (FFU) assay. Mice were infected between 8 and 12 weeks of age. Animals were anesthetized by intraperitoneal injection of ketamine/xylazine (10% (v/v) of 100 mg/mL ketamine and 5% (v/v) of 20 mg/mL xylazine in 0.9% (w/v) NaCl with a dose adjusted to body weight (200 μL/20 g body weight). Infection was performed by intranasal application of virus solution in 20 μL sterile phosphate-buffered saline (PBS), with a PR8M dosage of 2×10^3 FFU. Mice were infected in an approved animal facility at UTHSC or HZI.

2.3. Quantifying effects of infection on body weight and Trim21 expression

We calculated body weight loss at 3, 5, 8 and 14 d.p.i. of parental B6 and D2 mice that were also used for RNAseq analysis as a percentage of their initial weight. Mice that lost more than 30 % of their starting body weight were sacrificed for ethical reasons. We used the *Pearson correlation* coefficient to determine correlation between *Trim21* expression and body weight.

2.4. Data sets

B6D2-RNAseq: RNAseq data used here from parental strains have been described in our previous publication (Wilk et al., 2015; Xu et al., 2021)(GEO-ID: GSE 66,040). Briefly, mice were infected between 8 and 12 weeks of age by intranasal application of virus PR8M with a dose of 2×10^3 FFU. Lungs were collected on 1 and 3 days post infection (d.p.i) from mock-infected mice; 1, 3, and 5 d.p.i. from infected D2 mice; and 1, 3, 5, 8, and 14 d.p.i. from infected B6 mice, respectively, and processed for transcriptomics profiling by RNAseq. Reads were processed as described in (Wilk et al., 2015; Xu et al., 2021). Normalized, $\log_2$ transformed data are presented.

B6D2-RNAseq-BW: body weight changes from B6 and D2 mice from the B6D2-RNAseq experiment. Body weights were measured until 3 d.p.i. when mice were sacrificed for preparation of lung tissues for RNAseq analysis. Detailed data are provided in supplement ST1.

BXD-RNAseq: RNA-seq data from 41 BXD strains have been published previously by our group (Xu et al., 2021)(GEO-ID: GSE 165,744 and GeneNetwork ID: "HZI Lung Flu Infected BXD (Nov16) RNA-Seq"; GN807). Briefly, mice were infected between 8 and 12 weeks of age by intranasal application of virus PR8M with a dose of 2×10^3 FFU. RNA was prepared from lungs at 3 d.p.i. and sequenced. Reads were processed as described in (Wilk et al., 2015; Xu et al., 2021). Normalized, $\log_2$ transformed data are presented. Analysis and visualization of expression data was performed using the R software package (version 4.2.1) (R_Core_Team 2013a).

BXD-BW: The body weight changes from this experiment are provided in table ST2. Body weights were measured until 3 d.p.i. when mice were sacrificed for preparation of lung tissues for RNAseq analysis. Detailed data are provided in supplement ST2.

2.5. Expression quantitative trait locus (eQTL) mapping

Complex traits are the results of the expression of multiple genes, and chromosomal regions that are responsible for variances in the expression

traits can be revealed by eQTL mapping methods. To identify genetic loci that are responsible for regulating *Trim21* expression in BXD mice, we employed interval mapping method (Haley and Knott, 1992) to perform eQTL mapping using the lung dataset of "HZI Lung Flu Infected BXD (Nov16) RNA-Seq" that was previously published by us (Xu et al., 2021). This dataset is accessible through our GeneNetwork website (www.genenetwork.org) with the identifier GN807. The eQTL mapping was performed on GeneNetwork (www.genenetwork.org) using the interval mapping method (Haley and Knott, 1992). The interval or fast linear mapping method uses the likelihood ratio statistics (LRS) to measure the linkages between the investigated trait and genotype markers. The genome-wide significant and suggestive QTLs were determined with 1000 permutation tests. An LRS of 11.05 and 17.09 was considered as suggestive and significant threshold, respectively. This method used more than 7300 informative SNP genotype markers for the analysis; the file containing these genotype markers can be accessed through our GeneNetwork.

2.6. Genetic correlation analysis

We used *Pearson correlation* coefficient to identify genes that were co-expressed with *Trim21* in the lung transcriptome of BXD mice (BXD-RNAseq). We computed the *adjusted p-value* (Benjamini & Hochberg) for each correlation. Trim21-correlated genes having a correlation r of minimum ± 0.3 and a significance *p-value* <0.05 were selected for further analysis.

2.7. Candidate gene identification

A 2-LOD confidence interval within the eQTL region was used for identifying potential candidate genes modulating *Trim21* expression. We used a scoring system (scores ranging from 0 to 10) to prioritize the candidate genes. The scoring system contains five different parameters, and each parameter was assigned a different score based on its overall weightage.

1. **Mean expression in the lung dataset (1 score):** We considered genes with low expression levels (< 7) to be background noise. Hence genes with an expression of ≥ 7 in lung tissue were assigned a score of 1.
2. **Correlation with *Trim21* (2 score):** Genes significantly correlated ($p < 0.05$) with Trim21 were given higher weightage and were assigned a score of 2.
3. **Cis-regulation (1 score):** For the genes located within 2-LOD confidence interval, eQTL mapping was performed. A gene was considered *cis-regulated* and was assigned a score of 1, if the eQTL had >11 LRS and it was within 5 Mb of the gene's position.
4. **Coding SNP between D2 and B6 (1 score):** Genes harboring non-synonymous SNPs between B6 and D2 parental strains were assigned a score of 1.
5. **Functional relevance (5 score)**: To determine if the QTL genes are functionally important in lung infection, we used the following public databases: Mouse Genome Informatics (MGI, http://www.informatics.jax.org/) (Smith et al., 2018), Rat Genome Database (RGD, www.rgd.mcw.edu) (Smith et al., 2020), International Mouse Phenotyping Consortium (IMPC, http://www.mousephenotype.org/) (Dickinson et al., 2016), Gene Ontology (GO, http://geneontology.org) (Ashburner et al., 2000) and GWAS Catalog (www.ebi.ac.uk/gwas) (Buniello et al., 2019). These databases were queried with 'inflammation', 'flu', and 'immunity' related terms. Genes found in the RGD database and human GWAS portal were given a higher weightage of 4, whereas a score of 3 was assigned if found in other databases.

The scores across all the five categories were summed for each gene and those with a score of at least 5 (50 % of the total score) were selected as candidate genes for further analysis.

2.8. Gene set enrichment analysis

Genes that had significant correlation (sample correlation r of > 0.3 or < -0.3; $p < 0.05$ and literature correlation $r > 0.3$) with *Trim21* and having a mean expression value >7 were selected for gene set enrichment analysis (dataset BXD-RNAseq). We used *clusterProfiler* R package (Yu et al., 2012) for Kyoto Encyclopedia of Genes and Genomes (KEGG) (Kanehisa et al., 2002) pathway enrichment analyses with default parameters, while enriched mammalian phenotype ontologies (MPOs) were obtained using WebGestalt (www.webgestalt.org) (Liao et al., 2019) with 'protein coding genes' as the reference background and at least 5 genes in each category. Annotations with Benjamini-Hochberg corrected false discovery rate (FDR) *p-value* <0.05 were considered statistically significant.

2.9. Cells and IAV infection in vitro

HEK293FT, A549, and Vero cells were cultured in Dulbecco's Modified Eagle Medium (DMEM) supplemented with 10 % heat-inactivated fetal bovine serum, 100 I.U. of Penicillin, and 100 μg/mL Streptomycin, using conventional techniques. A nonstructural protein 1 (NS1)-truncated mutant IAV of H3N2 subtype, designated influenza A/swine/Texas/4199–2/98 1–126 (referred to as 1–126 TX/98) virus was provided by Richard Webby at St. Jude Children's Research Hospital, Memphis, TN (Solorzano et al., 2005). Virus stocks were prepared in the allantoic cavities of embryonated chicken eggs. Cells were infected with 1–126 TX/98 virus at the specified multiplicity of infection (MOI), or mock-infected, for the indicated times, prior to cell lysis for analyses of RNA and protein expression as described below.

2.10. RNA interference

To stably deplete TRIM21 expression, we employed a short hairpin RNA (shRNA) construct in pLKO.1-puro backbone specifically targeting human TRIM21 coding sequence (Openbiosystems, TRCN0000010839), which we found to be most effective in knocking down TRIM21 expression in preliminary testing of several shRNAs. The shRNA target sequence was GAGTTGGCTGAGAAGTTGGAA. The shRNA vector was packaged into replication-incompetent lentiviral particles in transfected HEK293FT cells, which were subsequently used to transduce A549 cells in the presence of 8 μg/ml polybrene (Sigma-Aldrich). Following selection in culture medium containing 1 μg/ml puromycin for ~7 days, surviving cells were pooled and used for analyses.

2.11. Quantitative RT-PCR

Total RNA was extracted from cells following indicated treatments using TRIzol (Invitrogen) and subsequently used to program cDNA synthesis using moloney murine leukemia virus (MMLV) reverse transcriptase (RT) (Promega) and random primers (Invitrogen) according to manufacturers' specifications. Quantitative real-time PCR was performed on the cDNA samples with gene-specific primers (see below), an Applied Biosystems SYBR green master mix and an Applied Biosystems QuantStudio 3 Real-Time PCR System. The primers for *IFNB1, IFNL1, CCL5, CXCL10, IFIT1*(a.k.a., *ISG56*), and *28S* (housekeeping internal control) have been described (Kumthip et al., 2017; Shen et al., 2012). Other primers used were: *IFIT3* (a.k.a., *ISG60*), 5′-TGAGGAAGGGTGGACACAACTGAA-3′ (forward) and

5′-AGGAGAATTCTGGGTTGTTGGGCT-3′ (reverse) (Li and Swaminathan, 2019); *MDA5* (a.k.a., *IFIH1*), 5′- CATCTGATTGGAGCTGGACA-3′

(forward) and

5′-TGCCACTGTGGTAGCGATAA-3′ (reverse); *RIG-I* (a.k.a, *DDX58*), 5′- GGACGTGGCAAAACAAATCAG-3′ (forward) and 5′-ATTGTGATCTC-CACTGGCTTTGA-3′ (reverse); and *TRIM21*, 5′-TCAGCAGCACGCTTGA-CAAT- 3′ (forward) and: 5′-GGCCACACTCGATGCTCAC-3′ (reverse) (Cheng et al., 2020). To monitor the level of 1–126 TX/98 virus replication, we used the following primers to gauge the intracellular expression of viral hemagglutinin (HA) mRNA: 5′-ACGAAATGGGA AAAGCTCAATAAT-3′ (forward) and 5′-CATTTGGAGTGATGCATTC AGAA-3′ (reverse). The relative abundance of transcript for each gene in each sample was normalized to that of *28S* ribosomal mRNA.

2.12. Immunoblotting

Cellular extracts were prepared, quantified for protein concentrations, and subjected to sodium dodecyl sulfate - polyacrylamide gel electrophoresis and subsequent Western blotting as described previously (Li, 2009). For immunodetection, we used the following monoclonal (mAb) and polyclonal (pAb) antibodies: mouse anti-IAV NP mAb 5/1 (Varich et al., 2009); Rabbit anti-TRIM21 mAb (Cell Signaling Technology); rabbit anti-IFIT1/ISG56 pAb (Wang et al., 2009); rabbit anti-IFIH1/MDA5 pAb (Proteintech); rabbit anti-DDX58/RIG-I pAb (Enzo Life Sciences); mouse anti-Vinculin mAb (Proteintech); and appropriate IRDye® secondary antibodies - goat anti-mouse IgG IRDye® 680RD or goat anti-rabbit IgG IRDye® 800CW (both from LI-COR Biosciences). Protein bands were visualized with an Odyssey infrared imaging system (LI-COR Biosciences). To compare the expression levels of a protein of interest across different samples in immunoblotting, signal intensity of the target protein band(s) was analyzed using Image Studio™ (LI-COR Biosciences) and normalized to that of a loading control, as specified.

2.13. IFN bioactivity assay

IFN production in cell culture supernatants, measured as antiviral bioactivity against vesicular stomatitis virus (Indiana strain), was determined by a micro-plaque reduction assay on Vero cells cultured in 96-well plates, as described (Langford et al., 1981). IFN titers were expressed as units/ml.

3. Results

3.1. Effects of IAV infection on Trim21 expression in the lungs of B6 and D2 mice at different time points following viral infection

B6 and D2 mice were mock-infected or challenged with IAV via the intranasal route. Basal expression of *Trim21* in mock-treated B6 and D2 was comparable. Following IAV challenge, the abundance of *Trim21* transcript was upregulated in both strains of animals (Fig. 1). Expression levels in D2 mice decreased strongly at 5 d.p.i. from 3 d.p.i. (although still much higher than 1 d.p.i.), most likely because of significant lung damage and mice being moribund (Srivastava et al., 2009). The extent to which Trim21 was upregulated in infected B6 mice was also slightly reduced on 8 d.p.i. compared with 3–5 d.p.i., concomitant with profound weight loss (see below in Fig. 2). Students' T-tests revealed that significant differences existed between mock-treated and infected lungs for both strains ($p = 2.53E\text{-}08$ for B6 and $p = 7.06E\text{-}08$ for D2, respectively). There was also a significant difference between the infected B6 and D2, with the latter having more heightened upregulation of *Trim21* expression on 3 d.p.i. ($p = 0.00288$, Fig. 1).

3.2. Effects of IAV infection on body weight in mice

Body weight of infected parental strains from which RNA was isolated for RNAseq analysis was recorded as percent of starting weight from the days of preparation (Fig. 2). D2 cases lost their weight quickly and progressively until 5 d.p.i. By comparison, infected B6 mice shed their mass more slowly and to a much lesser extent on 3 and 5 d.p.i., followed by recovering from their illness. By ~ 14 d.p.i., all B6 cases had regained their weight to nearly pre-infection levels (Fig. 2). There was a significant inverse correlation between animal body weight and *Trim21* expression levels (correlation coefficient: −0.6; significance: $p = 0.002$. $R^2 = 0.33$, Fig. 3).

3.3. Trim21 expression in the lungs of BXD mice

Trim21 expression was determined by RNAseq in 41 BXDs and both B6 and D2 parents in the lung dataset "HZI Lung Flu Infected BXD (Nov16) RNA-Seq" (GeneNetwork ID: GN807) (Xu et al., 2021). BXD56 had the lowest expression level (9.361) while BXD67 had the highest (9.842). The average expression of *Trim21* across the strains was 9.60 ±

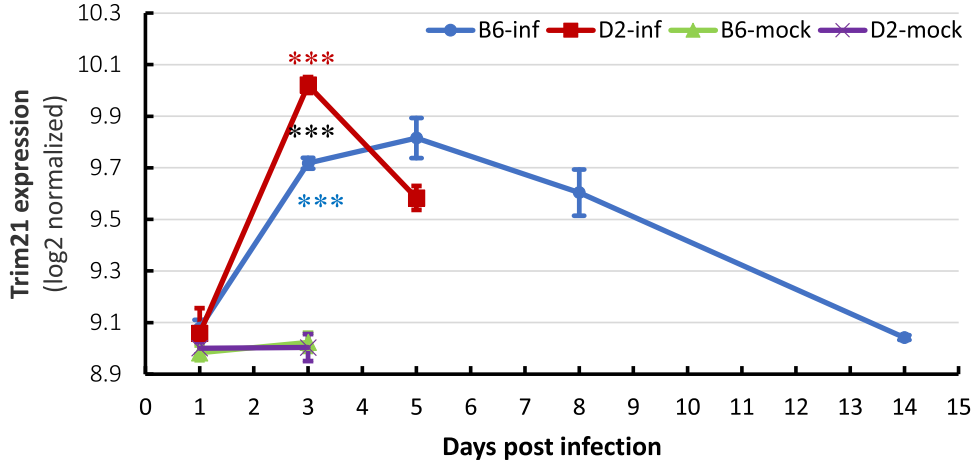

Fig. 1. Pulmonary *Trim21* expression at indicated time points post mock or IAV infection. The x-axis represents the days after infection, and the y-axis shows $\log_2$ normalized *Trim21* expression as a difference to expression levels on 0 d.p.i. (before infection). $n = 3$ mice per group. Note that D2 mice had to be sacrificed when losing more than 30 % of their starting body weight and, therefore only data for up to 5 d.p.i. were recorded for this strain. Data set: B6D2-RNAseq. Triple asterisks in red, blue, and black colors indicate $p < 0.001$ between infected and mock-infected D2, between infected and mock-infected B6, and between infected D2 and infected B6, respectively.

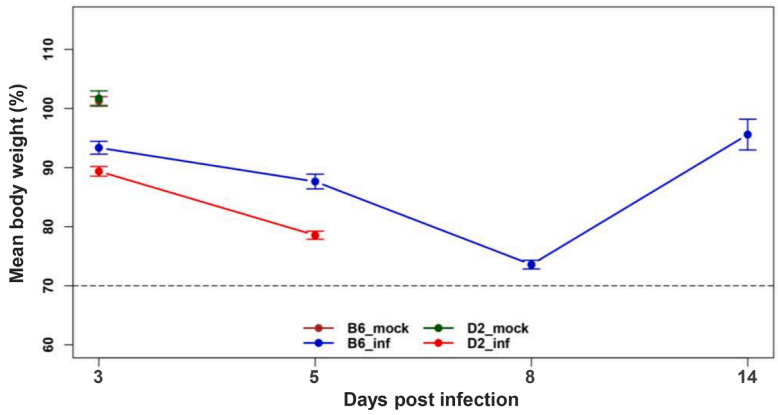

Fig. 2. Body weight changes of B6 and D2 mice post infection. The x-axis shows the days post infection, and the y-axis shows the mean body weight as a percentage (+/- 1 SEM) of the starting weight, which was set to 100 %. Body weight measurements are shown for days on which RNA was isolated for the RNAseq study. B6 mock: $n = 3$, B6 infected, $n = 12$ at 3 d.p.i., $n = 9$ at 5 d.p.i., $n = 6$ on 8 d.p.i. and $n = 3$ on 14 d.p.i.; D2 mock: $n = 3$, D2 infected, $n = 6$ on 3 d.p.i. and $n = 3$ on 5 d.p.i. Data set: B6D2-RNAseq-BW.

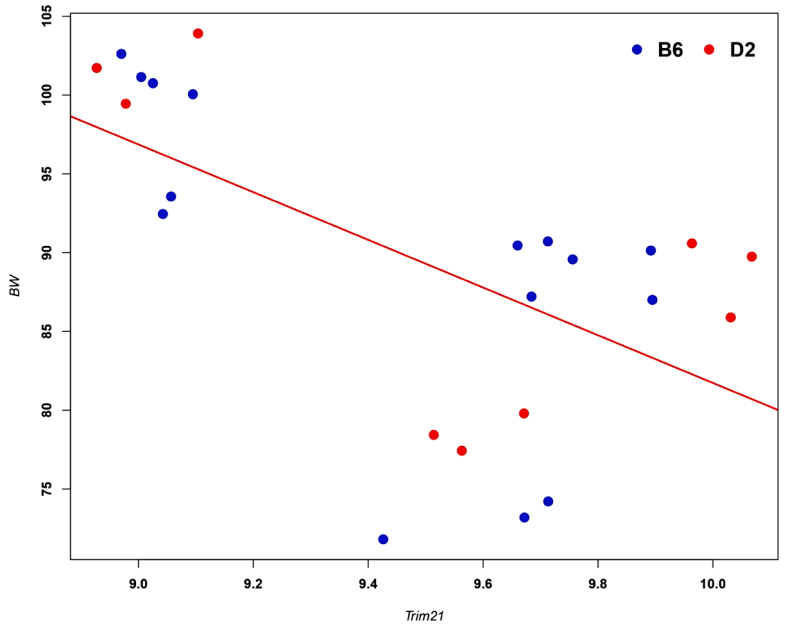

Fig. 3. Correlation analysis of body weight and *Trim21* gene expression. The x-axis shows the *Trim21* expression in $\log_2$-normalized expression values, the y-axis shows body weight as a percent of the starting weight. Data is shown for B6 and D2 mice from Fig. 2. Red line shows the modelled linear regression. B6 mock: $n = 3$, B6 infected, $n = 3$ at 3 d.p.i., $n = 3$ at 5 d.p.i., $n = 3$ on 8 d.p.i. and $n = 3$ on 14 d.p.i.; D2 mock: $n = 3$, D2 infected, $n = 3$ on 3 d.p.i. and $n = 3$ on 5 d.p.i. Data sets: B6D2-RNAseq, B6D2-RNAseq-BW.

0.10 (mean ± SD). We observed a 1.4-fold difference in *Trim21* expression across the BXDs and their parents (Fig. 4).

3.4. eQTL mapping

We performed eQTL mapping for *Trim21* expression in BXD mice and identified a significant eQTL on chromosome 14 (Chr 14) at 4∼10 Mb (peak LRS = 21.5 at 9.53 Mb) and two suggestive eQTLs at 19∼24 Mb (peak LRS = 15.4), and 114∼116 Mb (peak LRS = 13.6), respectively (Fig. 5) using interval mapping method in our GeneNetwork. These loci are distantly located from the genomic location of *Trim21* on chromosome 7 at 102.5 Mb (Fig. 5A), indicating that *Trim21* is trans-regulated.

3.5. Candidate gene identification

We considered a 2-LOD (one unit of LOD is equivalent to 4.61 units of LRS) interval for identifying the potential candidate genes modulating *Trim21* expression. The 2-LOD region ranged from 0∼24 Mb on Chr 14 covering the significant and one of the suggestive QTLs. This region contained a total of 54 genes. As described in the Methods section, we used a comprehensive scoring system to prioritize the candidate genes. Among 54 genes, 42 were expressed in IAV-infected mouse lungs (dataset "GN807: HZI Lung Flu Infected BXD (Nov16) RNA-Seq"), 4 were *cis-regulated*, 38 had significant correlation with *Trim21*, and 12 were identified as functionally relevant to immunity, inflammation or influenza based on data gathered from multiple resources. The potential candidate genes were ranked based on total score and finally 15 genes having a score of at least 5 (50 % of the total score) were selected for further analysis (Table 1).

To further investigate the 15 potential candidate genes and gain better insights into their association with viral infections, we examined existing literature for each gene's function in response to IAV infection, role in the immune system, and known relations to TRIM21. Our literature review supported two genes having functional relevance to

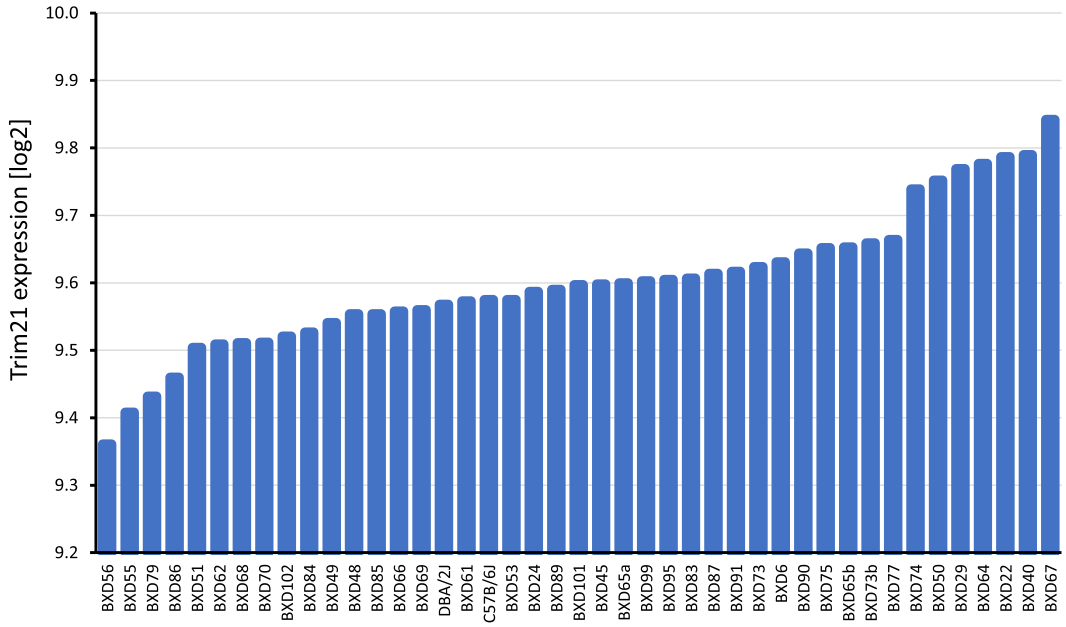

Fig. 4. Expression levels of *Trim21* in the lung tissue of IAV-infected BXD mice. The x-axis shows the indicated BXD strains and both parental strains, and the y-axis the $\log_2$-normalized expression levels of *Trim21*. Data set: BXD-RNAseq.

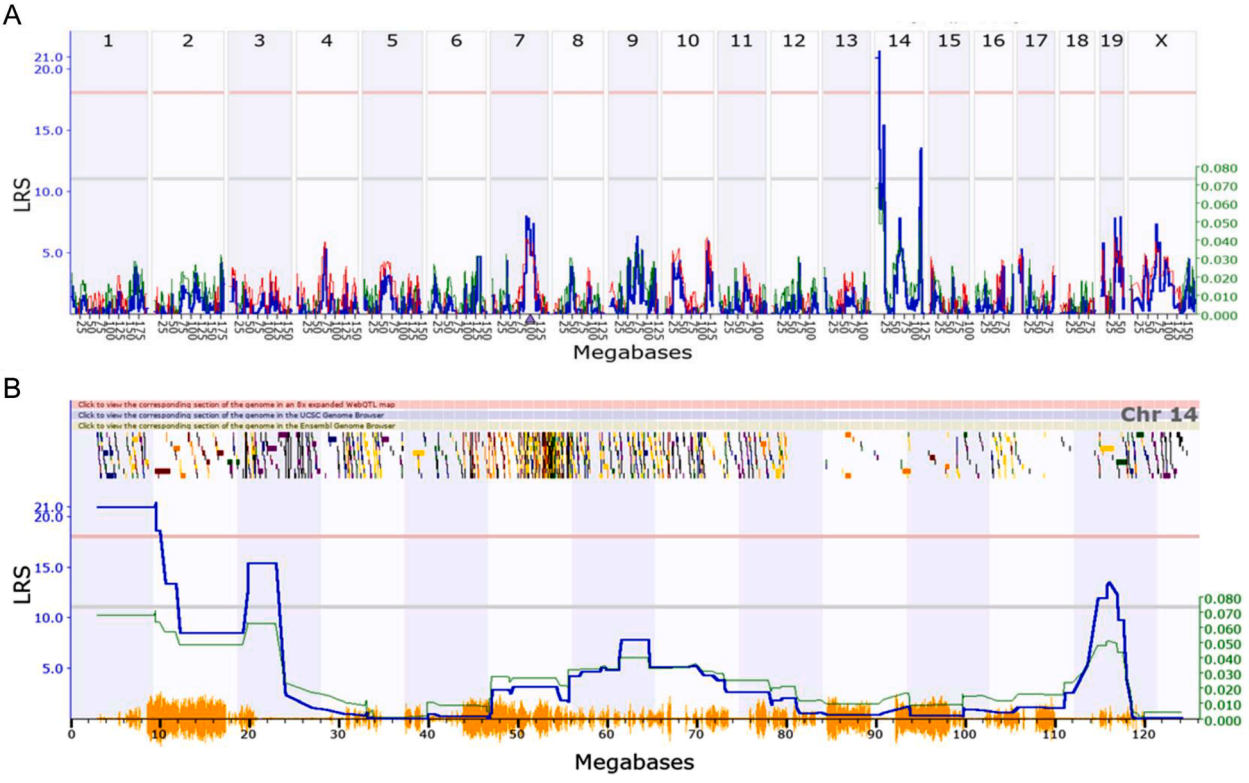

Fig. 5. Expression quantitative trait loci (eQTL) mapping for *Trim21* expression in BXD family. (A) Manhattan plot showing genome wide eQTL mapping in BXD mice. **(B)** Significant trans-eQTL mapped on chromosome 14. The x-axis denotes the chromosomal position in megabases on the mouse genome or chromosome 14, and y-axis indicates the LRS value. The red and blue horizontal lines indicate significant and suggestive thresholds, respectively. A SNP density plot is displayed along the x-axis in orange in panel B. Statistically significant eQTLs were identified at 4~10 Mb, and suggestive eQTLs at 19~24 Mb and 114~116 Mb on Chr 14. The genomic location of *Trim21* on chromosome 7 is indicated with a triangle in panel A. Data set: BXD-RNAseq.

Table 1
List of potential candidate genes in eQTL region and with a score of at least 5.

Gene symbol	Gene ID	Mean expression	Trim21 correlation	Non-synonymous SNP	Cis-regulation	Functional relevance	Total score
3830406C13Rik	218,734	1	2	1	1	–	**5**
Ptprg	19,270	1	2	1	1	–	**5**
Il3ra	16,188	1	2	1	1	–	**5**
Top2b	21,974	1	2	1	–	3	**7**
Nr1d2	353,187	1	2	1	–	3	**7**
Anxa7	11,750	1	–	1	–	3	**5**
Plau	18,792	1	2	–	–	4	**7**
Zfp503	218,820	1	2	–	–	3	**6**
Kcnma1	16,531	–	2	–	–	3	**5**
Dlg5	71,228	1	2	–	–	3	**6**
Polr3a	218,832	1	2	–	–	3	**6**
Abcc4	239,273	1	–	1	–	4	**6**
Dnajc3	100,037,258	1	2			4	**7**
Uggt2	66,435	1	2	1	1	–	**5**
Oxgr1	239,283		2	1		4	**7**

TRIM21 and IAV response, NR1D2 and IL3RA. NR1D2 has been implicated in circadian rhythm, which is known to regulate the immune system, while IL3RA is known to be directly involved in the immune system.

3.6. Gene set enrichment analysis of Trim21-correlated genes

To understand the function of TRIM21 in IAV-infected BXD mice lungs, we performed gene set enrichment analyses of the co-expressed genes. For this analysis, a total of 3456 *Trim21*-coexpressed genes that showed significant correlation (*correlation* $r > 0.3$ or < -0.3; $p < 0.05$), higher expression in lung (mean expression >7), and literature correlation >0.3 were considered. The enrichment analysis resulted in 106 significant (*adjusted* $p < 0.05$) KEGG pathways and 196 MPOs (**Supplementary Table 3**). Furthermore, we filtered the pathways based on the gene expression difference between virus-infected and mock-infected mice. The criteria were: a) over 20 % of pathway genes with significant FDR in infected mice on Day 3 compared to mock infected, and b) over 50 % of pathway genes with significant FDR in day 5 infected mice compared to mock infected. This resulted in 13 KEGG pathways, six of which are signaling pathways implicated in immunity, viral infections, and inflammation, one is Influenza A, and six are diseases with known effects on inflammation and immunity (Fig. 6A). Top 25 MPOs, many of which are related to immune system response and blood cell physiology are shown in Fig. 6B.

3.7. Depletion of TRIM21 augmented IAV-induced expression of key genes in innate antiviral immune response

We sought to experimentally validate if TRIM21 has a role, as predicted in our model, in IAV-elicited host responses. The adenocarcinomic human alveolar epithelial cell line, A549, has been widely used to model responses of lung epithelial cells to respiratory viruses including IAVs. To examine the impact of TRIM21 expressed at physiological levels, we created A549 cells with stable knockdown of TRIM21 using an shRNA specifically targeting *TRIM21* coding sequence (referred to as shT21).

We then mock-infected and infected A549 TRIM21-knockdown cells (A549-shT21) and control A549 cells, respectively, with IAV 1–126 TX/98 virus, and performed qRT-PCR to measure the abundance of mRNAs for *TRIM21, IFNL1, IFNB1, CCL5, CXCL10, IFIT1, IFIT3, DDX58, IFIH1*, and IAV HA. Because IAV NS1 protein strongly inhibits host gene expression including those of critical innate immune responses (Krug et al., 2003), we chose to use an NS1-trucated mutant, 1–126 TX/98 virus, which elicits more potent host responses than wild-type IAV (Solorzano et al., 2005) and thus would allow for more sensitive detection of any effects TRIM21 may have. As shown in Fig. 7, IAV infection stimulated expression of *TRIM21* in control A549 cells by ~3-fold, consistent with TRIM21 itself being an ISG and typically upregulated in virus-infected cells. By contrast, this viral upregulation of *TRIM21* transcript was abrogated in shT21 cells, supporting efficient knockdown of TRIM21 was achieved. Indeed, highly efficient depletion of TRIM21 protein in A549-shT21 cells was confirmed by immunoblot analysis (Figure 8A, see below). We found the IAV induction of *IFNL1* and *IFNB1*, key antiviral effector cytokines in the respiratory tract, was significantly augmented in TRIM21-knockdown cells than in control A549 cells, as was that of two prominent inflammatory chemokines, *CCL5* and *CXCL10*. In line with these observations, the IAV induction of multiple well-characterized ISGs, including *IFIT1* and *IFIT3*, and the cytosolic viral RNA sensors *DDX58* and *IFIH1* was also significantly enhanced in shT21 cells in comparison with control A549 cells. In these experiments, robust viral replication, as gauged by high levels of intracellular HA mRNA, was observed in both shT21 and control A549 cell lines; a barely ~2-fold drop in HA mRNA abundance was witnessed in the former than the latter (Fig. 7).

Next, we determined whether the effects of TRIM21 depletion on transcripts for host innate immune genes correlated with changes in their respective proteins, focusing on those critically involved in antiviral responses. Immunoblot analyses demonstrated expression of DDX58, IFIH1, and IFIT1 proteins was all substantially upregulated in control A549 cells at 17 h post-infection by IAV 1–126 TX/98 virus, but to greater extent in A549-shT21 cells (Fig. 8A, compare lanes 6 vs 3). Using an IFN bioactivity assay based on plaque reduction in vesicular stomatitis virus, a negative-strand RNA virus highly sensitive to the antiviral action of IFNs, we quantified IFN production in culture supernatants from IAV-challenged cells (Fig. 8B-C). It was revealed that A549-shT21 cells produced significantly higher amounts of IFN than control A549 cells.

Taken collectively, our mRNA and protein data consistently demonstrate that TRIM21 is a negative regulator of innate antiviral immune responses elicited by IAV in human alveolar epithelial cells.

4. Discussion

In this study, we took a systems genetics approach to extract key nodes in host responses to IAV infection. Our data suggest that a TRIM21-assoicated gene network contributes to orchestrating the innate immune mechanisms elicited by the virus, in ways that modulate IAV disease pathogenesis in mice. Specifically, we found *Trim21* to be differentially expressed between the BXD parents and across BXD RI strains that develop illness of varying severity, as judged by extent of weight loss, following IAV challenge (Nedelko et al., 2012). Of note, in IAV-infected mice viral replication starts at 1 d.p.i., reaches peak levels at ~ 5 d.p.i., and declines thereafter, becoming undetectable at ~7–8 d.p.i. Expression of IFNs, chemokines and cytokines follows this kinetics. The adaptive immune response starts at ~6–8 d.p.i. Recovery of disease

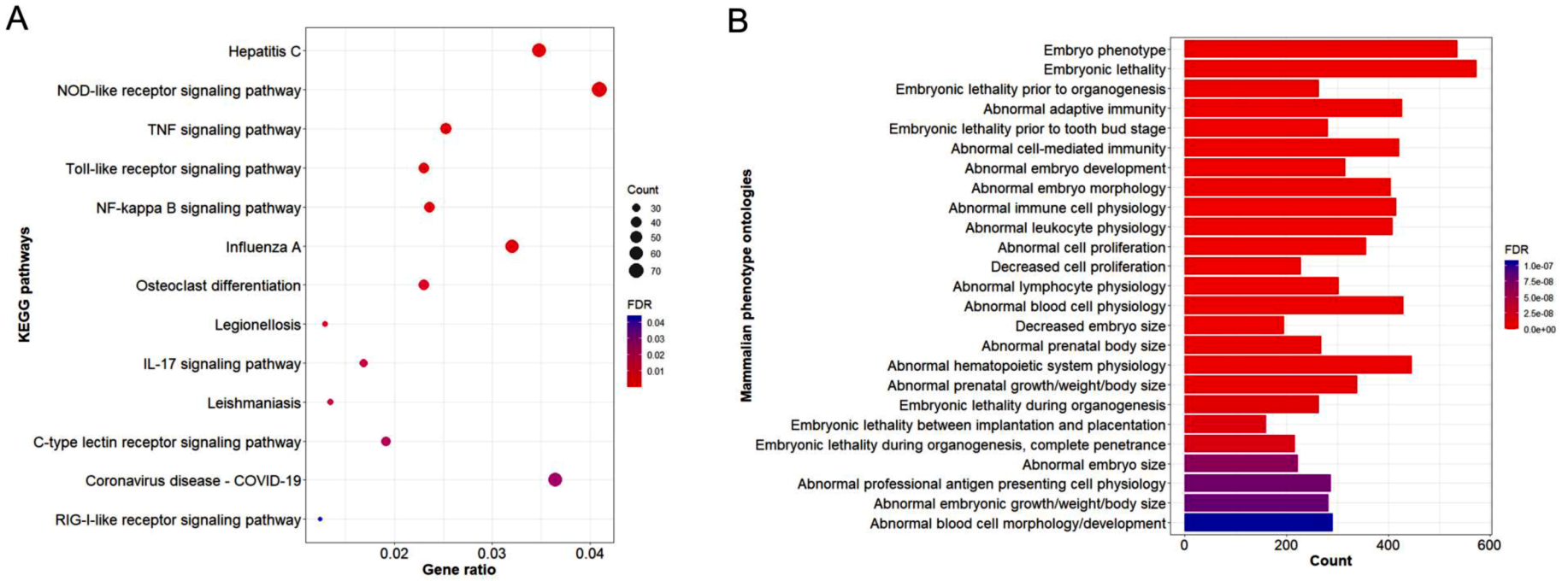

Fig. 6. Functional enrichment analysis of *Trim21*-correlated genes in IAV-infected BXD mice lung tissue. (A) Selected KEGG pathways, (B) top 25 MPOs enriched with *FDR corrected* $p < 0.05$. The x-axis shows gene ratio/count, and the y-axis shows enriched pathways/ontology terms. The R package *ggplot2* was used for constructing the plots. Data set: BXD-RNAseq.

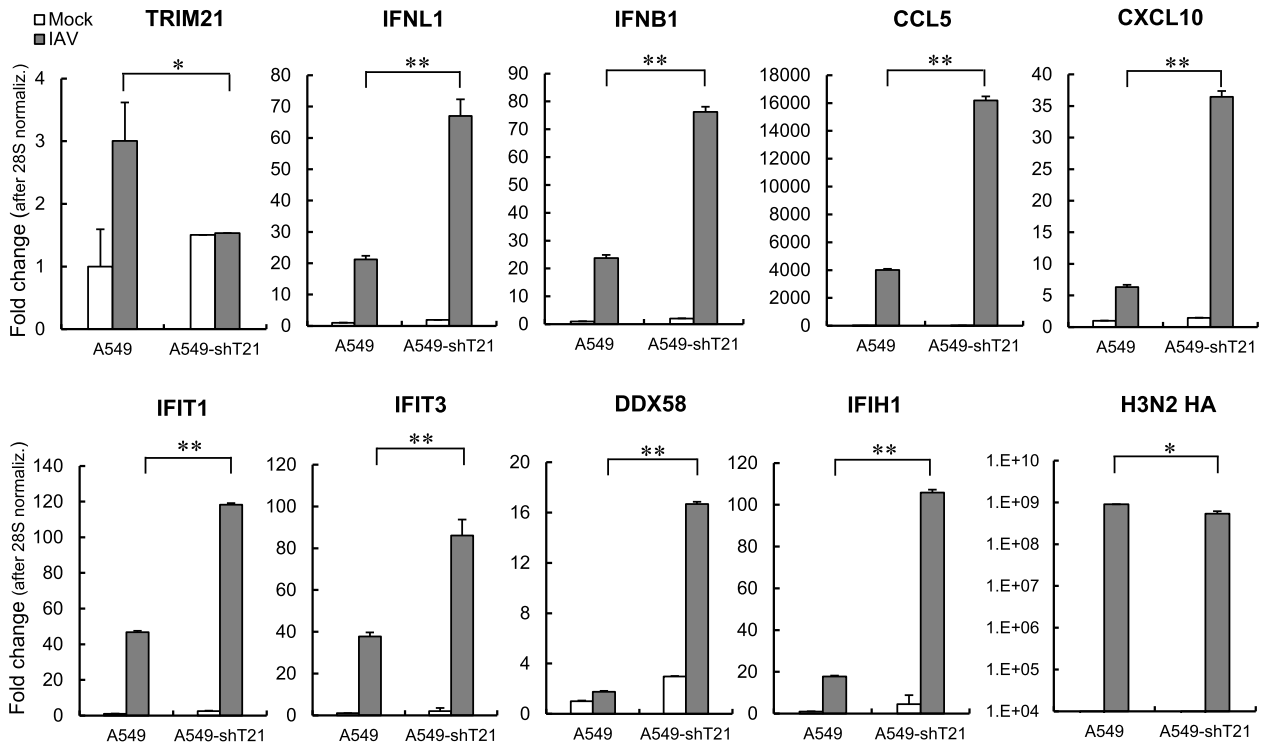

Fig. 7. Effects of TRIM21 knockdown on expression of innate immune genes transcripts in IAV-infected human lung adenocarcinoma epithelial cells. qRT-PCR analysis of *TRIM21, IFNL1, IFNB1, CCL5, CXCL10, IFIT1, IFIT3, DDX58, IFIH1*, and IAV HA mRNAs in control A549 cells and TRIM21-knockdown cells (shT21), mock-infected or infected by IAV 1–126 TX/98 for 20 h at an MOI of 3, respectively. Data are representative of three independent experiments and expressed as fold change (mean ± SD) relative to mock-infected control A549 cells after normalization by 28S. Student's T-test was used to compare the indicated groups for the presence of statistical significance (* and ** denote $p<0.05$ and $p<0.01$, respectively).

(regaining body weight) begins at ~8 d.p.i (Srivastava et al., 2009). We observed that the kinetics of pulmonary *Trim21* expression (Fig. 1) followed those of IAV presence and innate immune response. Therefore, we concentrated in our study on the early times post infection because we thought that these are most relevant for TRIM21 functions described herein. Our analyses revealed that *Trim21* transcript was upregulated to significantly greater extent in the highly susceptible D2 mice than in the relatively resistant B6 animals at 3 d.p.i., and that there was an inverse correlation between *Trim21* expression level and body weight, lending support for the notion that early, heightened induction of TRIM21 is associated with more severe disease in IAV-infected mice.

In addition, we characterized the molecular mechanism of TRIM21 regulation during IAV infection. Using eQTL mapping, we showed *Trim21* to be trans-regulated and identified 3 genomic regions on chromosome 14 containing ~54 potential candidate regulators. By analyzing the genomic expression data of 44 BXD RI lines and the parental strains, we identified genes co-expressed with *Trim21* and constructed a genetic network. After ranking potential candidates with a scoring system that took into consideration expression data, *Trim21* correlation, regulation, and functional relevance, we came down to a refined network comprising 15 highest-scoring genes. Within this network, IL3RA and NR1D2 are implicated in the immune system and inflammation. Based on their annotated roles and those described in literature, we propose these genes interact with TRIM21 to modulate the host's responses to influenza that may impact disease susceptibility and severity.

IL3RA is a subunit of interleukin receptor 3 (IL-3). In the presence of IFN beta (IFN-β), IL-3 leads to increased number of dendritic cells by preventing their apoptosis (Buelens et al., 2002). The resulting IL-3-IFN-β dendritic cells produce large amounts of IFN-α (Buelens et al., 2002). IFN-α stimulation up-regulates TRIM21 expression at the mRNA level (Strandberg et al., 2008). However, our data revealed a negative correlation ($r=-0.5291$) between IL3RA and TRIM21, which is counterintuitive to the reported mechanism by which IL3RA enhances TRIM21 expression. This may be reconciled by IL-3′s role in amplifying inflammation. Studies found IL-3 to cause flu-like side effects including fever when used in cancer treatment (Gerhartz et al., 1996). Perhaps IL-3 signaling is suppressed as a part of the body's protective response to avoid septic shock, as blocking IL-3 was found to reduce sepsis-induced mortality in mice (Weber et al., 2015).

NR1D2 is involved in the regulation of the circadian rhythm, which affects mental, physical, and behavioral aspects of mammals throughout the day, among which includes regulatory mechanisms of the immune system. Deletion of *Nr1d2* has been found to up-regulate *Bmal1* expression (Ikeda et al., 2019), which suppresses pro-inflammatory cytokines TNF-a and IL-6 (Oishi et al., 2017). Our data found positive correlation ($r=0.3596$) between NR1D2 and TRIM21, which supports a role for NR1D2 in IAV infection, but its relationship with TRIM21 is unclear. Previous research has indicated that toll-like receptors (TLR) are expressed rhythmically depending on the circadian clock (Baxter and Ray, 2020). TRIM21 activation by tyrosine phosphorylation was found to occur after TLR3 and TLR4 stimulation (Stacey et al., 2012). It is possible that TRIM21 is regulated downstream of TLR3 and TLR4, which are expressed based on the circadian cycle governed by NR1D2.

Our pathway enrichment analysis resulted in six signaling pathways relevant to IAV infection: TLR (Lee et al., 2013), IL-17 (Crowe et al., 2009), TNF (Salomon et al., 2007), C-type lectin receptor (Palomino-Segura et al., 2019), NF-kB (Bergmann and Elbahesh, 2019), and RLR (Ichinohe, 2010). Of these, NF-kB and RLR pathways were predicted to be regulated by TRIM21. siRNA depletion of TRIM21 in adenovirus type 5-infected human lung fibroblasts led to significantly diminished NF-kB expression and antiviral response (McEwan et al., 2013). Loss of TRIM21 also resulted in delayed immune response in cells infected with adenovirus and rhinovirus (Watkinson et al., 2015). TRIM21 targets IRF7, a master regulator of IFN-a production, for ubiquitination and proteasomal degradation during Sendai virus infection

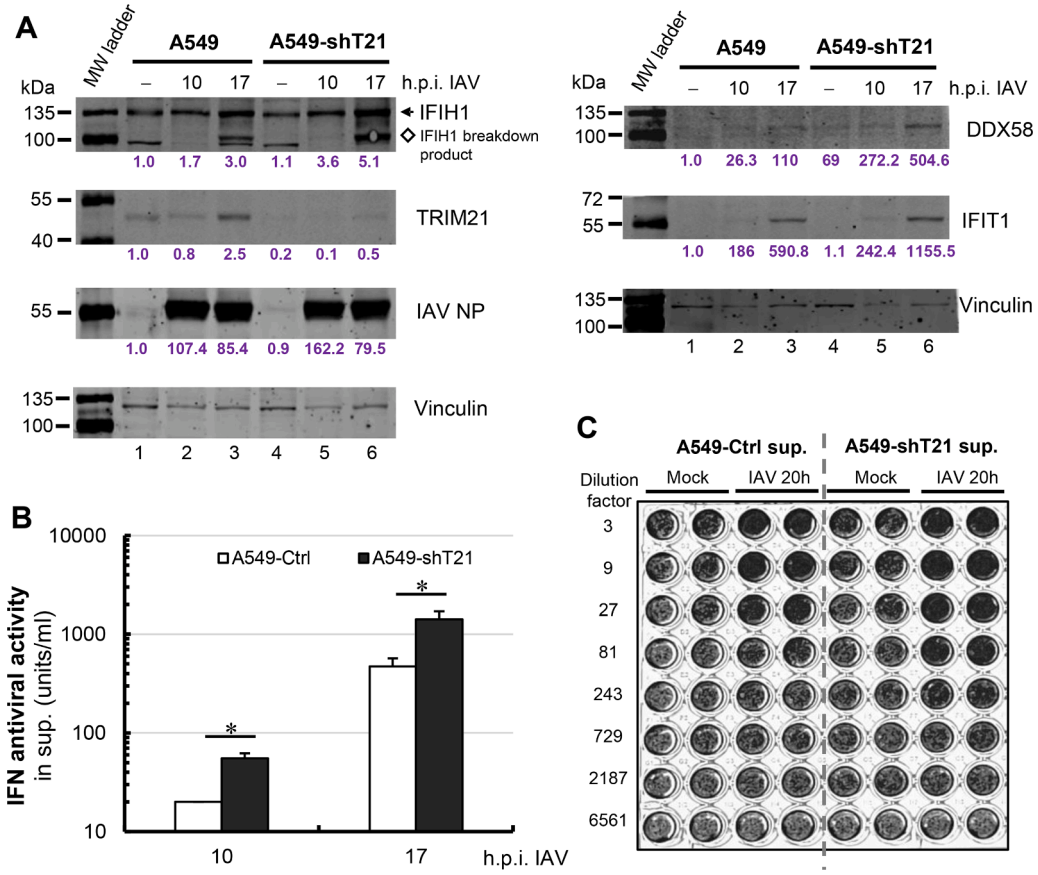

Fig. 8. Impact of TRIM21 depletion on expression of ISG proteins and IFN production in IAV-infected human lung adenocarcinoma epithelial cells. (A) Expression of TRIM21, IFIT1/ISG56, DDX58/RIG-I, IFIH1/MDA5, Vinculin (loading control), and IAV NP proteins in control A549 cells and TRIM21-knockdown cells (A549-shT21), mock-infected or infected by IAV 1–126 TX/98 (MOI = 2) for the indicated times. Data are representative of three independent experiments. Note that at 17 h.p.i., a breakdown product of IFIH1 protein (marked by diamond) was also detected and more so in shT21 cells (lane 6) than in control A549 (lane 3). Numbers in purple color under each target blot denote relative expression of the protein of interest after normalization to Vinculin loading control analyzed by Image Studio™ (LI-COR biosciences). (B) IFN production, as measured by antiviral activity present in culture supernatants under the indicated conditions. Data are compiled from two independent experiments and expressed as units/ml. Student's T-test was used to compare the indicated groups for the presence of statistical significance (* denotes $p<0.05$). A representative crystal violet staining of the plaque-reduction assay cell plate from two independent experiments is shown in (C). Mock, culture supernatant of mock-infected cells; IAV 20 h, culture supernatant of cells infected by IAV 1–126 TX/98 (MOI=3) for 20 h.

(Young et al., 2011). However, data on its effect on IRF3 and associated downstream events have been contradictory (reviewed in (Jones et al., 2021)). Moreover, whether TRIM21 affects these signaling pathways in the context of IAV infection is unclear. Given that IAV infection is predominantly sensed by RIG-I (a.k.a., DDX58) in epithelial cells, fibroblasts, and conventional dendritic cells (Kato et al., 2006), we strived to determine whether TRIM21 may impact RLR-mediated innate immune mechanisms against the virus. Our loss-of-function experiments in cultured human lung epithelial A549 cells based on RNAi depletion approach demonstrated that endogenously expressed TRIM21 negatively regulates IAV-induced expression of key antiviral cytokines (IFNB1 and IFNL1) and inflammatory chemokines (CCL5 and CXCL10), all of which hinge on coordinated activation of IRF3 and NF-kB transcription factors (Honda et al., 2005; Onoguchi et al., 2007; Genin et al., 2000; Brownell et al., 2014). This also holds true when it comes to induction of well-characterized antiviral ISGs including IFIT1, IFIT3, DDX58, and IFIH1, as supported by our data. Importantly, the heightened IFN response phenotype after TRIM21 depletion was corroborated at the protein level, as determined by IFN production in culture supernatants and intracellular expression of ISG proteins. Precisely how TRIM21 puts a check on RIG-I signaling that culminates in induction of these key genes as part of the innate immune responses to IAV infection will require further study.

While the focus of our study was on the impact of TRIM21 on host responses to IAV, we did observe TRIM21 depletion was associated with a moderate reduction in replication (as gauged by HA mRNA production) of IAV 1–126 TX/98, an H3N2 virus, in A549 cells (Fig. 7). Interestingly, Ouyang et al. observed knockdown of TRIM21 decreased IAV PR8 (an H1N1 virus) titers in infected A549 cells when they investigated how N-myc and STAT interactor (NMI) facilitated IAV infection (Ouyang et al., 2021). These authors reported overexpression of NMI led to IRF7 polyubiquitination and subsequent proteosomal degradation, an effect partially reversed by TRIM21 knockdown. Their study, however, did not examine if silencing TRIM21 affected cellular innate immune responses to IAV infection. Given that TRIM21 participates in IAV-induced autophagy (Sparrer et al., 2017), a catabolic pathway that is proviral for IAV (Zhou et al., 2009), it remains to be determined regarding the precise mechanism(s) by which TRIM21 supports IAV infection, i.e., how much it pertains to the protein's activity in promoting autophagy and to what extent it involves the negative regulation of innate antiviral responses. Surprisingly and currently not understood, contrary to our finding in this study and that of Ouyang et al. (Ouyang et al., 2021), Lin et al. recently reported TRIM21 exerted antiviral effects against IAVs of H3/H5/H9 subtypes but not those of H1/H7 subtypes (Lin et al., 2023). Future studies are needed to address whether this discrepancy stems from different viral strains tested or perhaps differences in experimental conditions.

The three pathways having the highest percentage of genes with

significant difference in expression between IAV-infected and mock-infected mice were the TLRs, TNF, and COVID-19. TLRs are expressed by many different cell types that occupy or patrol the lungs and their recognition of various viral pathogen-associated molecular patterns can modulate the early innate immune responses, thereby impacting disease outcomes (Lester and Li, 2014). Three TLRs are known to engage with and be activated during IAV infection: TLR3, TLR7 and TLR8 (Guillot et al., 2005; Zhao et al., 2012). In line with this, intranasal pretreatment of mice with poly(I:C), a TLR3 agonist, and to lesser degrees, TLR9, TLR7/8, or TLR4 agonists, was shown to protect animals against lethal IAV challenge and reduce viral loads and lung pathology (Zhao et al., 2012). In neutrophils, TLR7 and TLR8 interactions with IAV RNA is necessary for proinflammatory cytokine production (Wang et al., 2008). TLR3 also is activated during IAV infection, although conflicting data, dependent on infection settings, have been reported, documenting either an antiviral protective role or a deleterious, proinflammatory one (Perales-Linares and Navas-Martin, 2013). Interestingly, there is a direct link between TLR3 and TLR4 stimulation and TRIM21 phosphorylation (Stacey et al., 2012). TNF has also been implicated in IAV infection. This NF-kB-dependent inflammatory cytokine is markedly upregulated in cultured cells and in mouse lungs following IAV infection. TNF pretreatment exerted potent antiviral activity against IAV in porcine lung epithelial cell cultures (Seo and Webster, 2002). However, it failed to do so in mice (Zhao et al., 2012), suggesting TNF mainly plays a proinflammatory role in vivo. Notably, TNF has also been shown to be regulated by TRIM21. Infection by mouse adenovirus resulted in a 50-fold increase of TNFα expression in wild-type cells but did not have a significant effect in *Trim21* knockout mice (Watkinson et al., 2013). Given some shared aspects of host innate immunity against IAV and SARS coronavirus (Zhao et al., 2012), it was not a total surprise that the coronavirus response pathway was among those emerged from our analyses - a majority of genes with a significant FDR difference between infected and mock infected groups (*Ifih1, Oas1b, Stat1, Ccl12, Mx2, Stat2, Ddx58, Oas2, C3, Irf9, Ikbke*) were also involved in the Influenza-A pathway. The exceptions were *Cybb* and *C2*. *Cybb* is a component of microbicidal phagocyte NADPH oxidase, while *C2* encodes the C2 protein which forms a part of the complement system and is associated with autoimmune diseases. Absence of *Cybb* has been found to increase viral clearance and lung function and reduce lung damage (Snelgrove et al., 2006), but it is unknown whether *C2* is linked to influenza pathogenesis. Since neither of these genes has been found to regulate TRIM21, we favor the hypothesis that the TLR pathway is most likely involved in the regulation of TRIM21 in the context of IAV infection.

In summary, our study suggests a TRIM21-associated gene network participates in modulating pulmonary innate immune responses to and pathogenesis of IAV in mice. Additionally, we demonstrate that TRIM21 negatively impacts the induction of key antiviral and inflammatory genes via the RLR pathway in a human airway epithelial cell culture model of IAV infection.

4.1. Limitations of this study

We have experimentally verified a negatively regulatory role of TRIM21 in innate immune responses to IAV in a human alveolar epithelial cancer cell line A549 challenged by an H3N2 subtype of IAV, as suggested by computational modeling of body weight and lung transcriptome data from mice infected with IAV-PR8M (a mouse adapted PR8 virus of H1N1 subtype). How much this is the case with other IAV subtypes (or even strains) will require further study. It should also be noted that the early host responses to IAV in vivo are complex and may be differently regulated by TRIM21 across cell types, and that influenza susceptibility/severity is a net result of the cross-talks and interactions among different cell types and signaling pathways. Outstanding is the question of to what extent the TRIM21 axis contributes to regulating the balance between protective antiviral host responses reining in IAV replication and harmful inflammatory reactions exacerbating pathological changes. Thus, future studies in TRIM21-deficient animal models are warranted to clarify the exact physiological impact of this protein and its co-regulators on IAV-host interactions and disease outcome.

Supplements

Table ST1. B6D2-RNAseq-BW. Body weight changes for B6 and D2 mice from the B6D2-RNAseq experiment.

Table ST2. BXD-BW. Body weight changes for BXD mice from the BXD-RNAseq experiment.

Table ST3. KEGG&MPO. All significant (*adjusted* $p < 0.05$) KEGG pathways and MPOs.

CRediT authorship contribution statement

Zhuoyuan Alex Li: Investigation, Formal analysis, Writing – original draft, Visualization, Funding acquisition. **Akhilesh Kumar Bajpai:** Software, Formal analysis, Data curation, Writing – original draft. **Ruixue Wang:** Validation, Investigation. **Yaxin Liu:** Validation, Investigation. **Richard J. Webby:** Resources. **Esther Wilk:** Investigation. **Weikuan Gu:** Supervision. **Klaus Schughart:** Methodology, Data curation, Writing – review & editing, Funding acquisition. **Kui Li:** Conceptualization, Methodology, Validation, Formal analysis, Resources, Writing – review & editing, Supervision, Project administration. **Lu Lu:** Conceptualization, Methodology, Formal analysis, Data curation, Resources, Writing – review & editing, Supervision, Project administration.

Declaration of competing interest

The authors declare that they have no known competing financial interests or personal relationships that could have appeared to influence the work reported in this paper.

Data availability

The datasets presented in this study can be found in online repositories. The names of the repository/repositories and accession number(s) are at https://www.genenetwork.org/ (GN807), https://www.ncbi.nlm.nih.gov/ (GSE165744), https://www.ncbi.nlm.nih.gov/ (66040).

Acknowledgement

This study was supported in part by start-up funding from UTHSC, intramural grants from the Helmholtz-Association (Program Infection and Immunity), and NIAID Research Grants 2-U19-AI100625–06 REVISED and 5U19AI100625–07 awarded to KS. K.R.S. is supported by NHMRC investigator grant 2007919. Z.A.L. is a UTHSC Summer Research Scholar. The funders had no role in study design, data collection and analysis, decision to publish, or preparation of the manuscript.

Supplementary materials

Supplementary material associated with this article can be found, in the online version, at doi:10.1016/j.virusres.2024.199335.

References

Ashburner, M., Ball, C.A., Blake, J.A., Botstein, D., Butler, H., Cherry, J.M., et al., 2000. Gene ontology: tool for the unification of biology. The Gene Ontology Consortium. Nat. Genet. 25 (1), 25–29. https://doi.org/10.1038/75556. PubMed PMID: 10802651; PubMed Central PMCID: PMCPMC3037419.

Baxter, M., Ray, D.W., 2020. Circadian rhythms in innate immunity and stress responses. Immunology 161 (4), 261–267. https://doi.org/10.1111/imm.13166. Epub 20200103PubMed PMID: 31820826; PubMed Central PMCID: PMCPMC7692257.
Bergmann, S., Elbahesh, H., 2019. Targeting the proviral host kinase, FAK, limits influenza a virus pathogenesis and NFkB-regulated pro-inflammatory responses. Virology 534, 54–63. https://doi.org/10.1016/j.virol.2019.05.020. Epub 20190601PubMed PMID: 31176924.
Boon, A.C., deBeauchamp, J., Hollmann, A., Luke, J., Kotb, M., Rowe, S., et al., 2009. Host genetic variation affects resistance to infection with a highly pathogenic H5N1 influenza A virus in mice. J. Virol. 83 (20), 10417–10426. https://doi.org/10.1128/JVI.00514-09. Epub 2009/08/27PubMed PMID: 19706712; PubMed Central PMCID: PMCPMC2753106.
Brownell, J., Bruckner, J., Wagoner, J., Thomas, E., Loo, Y.M., Gale Jr., M., et al., 2014. Direct, interferon-independent activation of the CXCL10 promoter by NF-kappaB and interferon regulatory factor 3 during hepatitis C virus infection. J. Virol. 88 (3), 1582–1590. https://doi.org/10.1128/JVI.02007-13. Epub 20131120PubMed PMID: 24257594; PubMed Central PMCID: PMCPMC3911583.
Buelens, C., Bartholome, E.J., Amraoui, Z., Boutriaux, M., Salmon, I., Thielemans, K., et al., 2002. Interleukin-3 and interferon beta cooperate to induce differentiation of monocytes into dendritic cells with potent helper T-cell stimulatory properties. Blood 99 (3), 993–998. https://doi.org/10.1182/blood.v99.3.993. PubMed PMID: 11807004.
Buniello, A., MacArthur, J.A.L., Cerezo, M., Harris, L.W., Hayhurst, J., Malangone, C., et al., 2019. The NHGRI-EBI GWAS Catalog of published genome-wide association studies, targeted arrays and summary statistics 2019. Nucleic. Acids. Res. 47 (D1), D1005–D1D12. https://doi.org/10.1093/nar/gky1120. PubMed PMID: 30445434; PubMed Central PMCID: PMCPMC6323933.
Cheng, J., Huang, Y., Zhang, X., Yu, Y., Wu, S., Jiao, J., et al., 2020. TRIM21 and PHLDA3 negatively regulate the crosstalk between the PI3K/AKT pathway and PPP metabolism. Nat. Commun. 11 (1), 1880. https://doi.org/10.1038/s41467-020-15819-3. Epub 20200420PubMed PMID: 32312982; PubMed Central PMCID: PMCPMC7170963.
Crowe, C.R., Chen, K., Pociask, D.A., Alcorn, J.F., Krivich, C., Enelow, R.I., et al., 2009. Critical role of IL-17RA in immunopathology of influenza infection. J. Immunol. 183 (8), 5301–5310. https://doi.org/10.4049/jimmunol.0900995. Epub 20090925PubMed PMID: 19783685; PubMed Central PMCID: PMCPMC3638739.
Dickinson, M.E., Flenniken, A.M., Ji, X., Teboul, L., Wong, M.D., White, J.K., et al., 2016. High-throughput discovery of novel developmental phenotypes. Nature 537 (7621), 508–514. https://doi.org/10.1038/nature19356. Epub 20160914PubMed PMID: 27626380; PubMed Central PMCID: PMCPMC5295821.
Genin, P., Algarte, M., Roof, P., Lin, R., Hiscott, J, 2000. Regulation of RANTES chemokine gene expression requires cooperativity between NF-kappa B and IFN-regulatory factor transcription factors. J. Immunol. 164 (10), 5352–5361. https://doi.org/10.4049/jimmunol.164.10.5352. PubMed PMID: 10799898.
Gerhartz, H.H., Zwierzina, H.H., Walther, J., Fenaux, P., Hayat, M., Jacobs, A., et al., 1996. Interleukin-3 plus low-dose cytosine arabinoside for advanced myelodysplasia: a pilot study. EORTC Leukemia Group. Cancer Invest. 14 (4), 299–306. https://doi.org/10.3109/07357909609012155. PubMed PMID: 8689423.
Guillot, L., Le Goffic, R., Bloch, S., Escriou, N., Akira, S., Chignard, M., et al., 2005. Involvement of toll-like receptor 3 in the immune response of lung epithelial cells to double-stranded RNA and influenza A virus. J. Biol. Chem. 280 (7), 5571–5580. https://doi.org/10.1074/jbc.M410592200. Epub 20041203PubMed PMID: 15579900.
Haley, C.S., Knott, S.A., 1992. A simple regression method for mapping quantitative trait loci in line crosses using flanking markers. Heredity (Edinb) 69 (4), 315–324. https://doi.org/10.1038/hdy.1992.131. PubMed PMID: 16718932.
Honda, K., Yanai, H., Takaoka, A., Taniguchi, T., 2005. Regulation of the type I IFN induction: a current view. Int. Immunol. 17 (11), 1367–1378. https://doi.org/10.1093/intimm/dxh318. Epub 20051007PubMed PMID: 16214811.
Ichinohe, T., 2010. Respective roles of TLR, RIG-I and NLRP3 in influenza virus infection and immunity: impact on vaccine design. Expert. Rev. Vaccines. 9 (11), 1315–1324. https://doi.org/10.1586/erv.10.118. PubMed PMID: 21087109.
Ikeda, R., Tsuchiya, Y., Koike, N., Umemura, Y., Inokawa, H., Ono, R., et al., 2019. REV-ERBalpha and REV-ERBbeta function as key factors regulating Mammalian Circadian Output. Sci Rep. 9 (1), 10171. https://doi.org/10.1038/s41598-019-46656-0. Epub 20190715PubMed PMID: 31308426; PubMed Central PMCID: PMCPMC6629614.
Jones, E.L., Laidlaw, S.M., Dustin, L.B., 2021. TRIM21/Ro52 - roles in innate immunity and autoimmune disease. Front. Immunol. 12, 738473 https://doi.org/10.3389/fimmu.2021.738473. Epub 20210906PubMed PMID: 34552597; PubMed Central PMCID: PMCPMC8450407.
Kanehisa, M., Goto, S., Kawashima, S., Nakaya, A., 2002. The KEGG databases at GenomeNet. Nucleic. Acids. Res. 30 (1), 42–46. https://doi.org/10.1093/nar/30.1.42. PubMed PMID: 11752249; PubMed Central PMCID: PMCPMC99091.
Kato, H., Takeuchi, O., Sato, S., Yoneyama, M., Yamamoto, M., Matsui, K., et al., 2006. Differential roles of MDA5 and RIG-I helicases in the recognition of RNA viruses. Nature 441 (7089), 101–105. https://doi.org/10.1038/nature04734. Epub 20060409PubMed PMID: 16625202.
Kimura, T., Jain, A., Choi, S.W., Mandell, M.A., Johansen, T., Deretic, V., 2017. TRIM-directed selective autophagy regulates immune activation. Autophagy 13 (5), 989–990. https://doi.org/10.1080/15548627.2016.1154254. PubMed PMID: 26983397; PubMed Central PMCID: PMCPMC5446080.
Kimura, T., Jain, A., Choi, S.W., Mandell, M.A., Schroder, K., Johansen, T., et al., 2015. TRIM-mediated precision autophagy targets cytoplasmic regulators of innate immunity. J. Cell Biol. 210 (6), 973–989. https://doi.org/10.1083/jcb.201503023. PubMed PMID: 26347139; PubMed Central PMCID: PMCPMC4576868.
Krug, R.M., Yuan, W., Noah, D.L., Latham, A.G., 2003. Intracellular warfare between human influenza viruses and human cells: the roles of the viral NS1 protein. Virology 309 (2), 181–189. https://doi.org/10.1016/s0042-6822(03)00119-3. PubMed PMID: 12758165.
Kumthip, K., Yang, D., Li, N.L., Zhang, Y., Fan, M., Sethuraman, A., et al., 2017. Pivotal role for the ESCRT-II complex subunit EAP30/SNF8 in IRF3-dependent innate antiviral defense. PLoS. Pathog. 13 (10), e1006713 https://doi.org/10.1371/journal.ppat.1006713. Epub 20171030PubMed PMID: 29084253; PubMed Central PMCID: PMCPMC5679654.
Langford, M.P., Weigent, D.A., Stanton, G.J., Baron, S., 1981. Virus plaque-reduction assay for interferon: microplaque and regular macroplaque reduction assays. Methods Enzymol. 78 (Pt A), 339–346. https://doi.org/10.1016/0076-6879(81)78139-4. PubMed PMID: 6173610.
Lee, N., Wong, C.K., Hui, D.S., Lee, S.K., Wong, R.Y., Ngai, K.L., et al., 2013. Role of human Toll-like receptors in naturally occurring influenza A infections. Influenza Other Respir. Viruses. 7 (5), 666–675. https://doi.org/10.1111/irv.12109. Epub 20130401PubMed PMID: 23552014; PubMed Central PMCID: PMCPMC5781199.
Lester, S.N., Li, K., 2014. Toll-like receptors in antiviral innate immunity. J. Mol. Biol. 426 (6), 1246–1264. https://doi.org/10.1016/j.jmb.2013.11.024. Epub 20131203PubMed PMID: 24316048; PubMed Central PMCID: PMCPMC3943763.
Li, D., Swaminathan, S., 2019. Human IFIT proteins inhibit lytic replication of KSHV: a new feed-forward loop in the innate immune system. PLoS. Pathog. 15 (2), e1007609 https://doi.org/10.1371/journal.ppat.1007609. Epub 20190219PubMed PMID: 30779786; PubMed Central PMCID: PMCPMC6396945.
Li, K., 2009. Regulation of interferon regulatory factor 3-dependent innate immunity by the HCV NS3/4A protease. Methods Mol. Biol. 510, 211–226. https://doi.org/10.1007/978-1-59745-394-3_16. PubMed PMID: 19009264.
Liao, Y., Wang, J., Jaehnig, E.J., Shi, Z., WebGestalt, Zhang B., 2019. 2019: gene set analysis toolkit with revamped UIs and APIs. Nucleic. Acids. Res. 47 (W1), W199–W205. https://doi.org/10.1093/nar/gkz401. PubMed PMID: 31114916; PubMed Central PMCID: PMCPMC6602449.
Lin, L., Wang, X., Chen, Z., Deng, T., Yan, Y., Dong, W., et al., 2023. TRIM21 restricts influenza A virus replication by ubiquitination-dependent degradation of M1. PLoS. Pathog. 19 (6), e1011472 https://doi.org/10.1371/journal.ppat.1011472. Epub 20230621PubMed PMID: 37343022; PubMed Central PMCID: PMCPMC10325077.
Mallery, D.L., McEwan, W.A., Bidgood, S.R., Towers, G.J., Johnson, C.M., James, L.C., 2010. Antibodies mediate intracellular immunity through tripartite motif-containing 21 (TRIM21). Proc. Natl. Acad. Sci. U.S.A. 107 (46), 19985–19990. https://doi.org/10.1073/pnas.1014074107. Epub 20101102PubMed PMID: 21045130; PubMed Central PMCID: PMCPMC2993423.
McEwan, W.A., Tam, J.C., Watkinson, R.E., Bidgood, S.R., Mallery, D.L., James, L.C., 2013. Intracellular antibody-bound pathogens stimulate immune signaling via the Fc receptor TRIM21. Nat. Immunol. 14 (4), 327–336. https://doi.org/10.1038/ni.2548. Epub 20130303PubMed PMID: 23455675; PubMed Central PMCID: PMCPMC3672961.
Nedelko, T., Kollmus, H., Klawonn, F., Spijker, S., Lu, L., Hessman, M., et al., 2012. Distinct gene loci control the host response to influenza H1N1 virus infection in a time-dependent manner. BMC Genomics 13, 411. https://doi.org/10.1186/1471-2164-13-411. Epub 2012/08/22PubMed PMID: 22905720; PubMed Central PMCID: PMCPMC3479429.
Oishi, Y., Hayashi, S., Isagawa, T., Oshima, M., Iwama, A., Shimba, S., et al., 2017. Bmal1 regulates inflammatory responses in macrophages by modulating enhancer RNA transcription. Sci. Rep. 7 (1), 7086. https://doi.org/10.1038/s41598-017-07100-3. Epub 20170801PubMed PMID: 28765524; PubMed Central PMCID: PMCPMC5539165.
Oke, V., Wahren-Herlenius, M., 2012. The immunobiology of Ro52 (TRIM21) in autoimmunity: a critical review. J. Autoimmun. 39 (1–2), 77–82. https://doi.org/10.1016/j.jaut.2012.01.014. Epub 20120307PubMed PMID: 22402340.
Onoguchi, K., Yoneyama, M., Takemura, A., Akira, S., Taniguchi, T., Namiki, H., et al., 2007. Viral infections activate types I and III interferon genes through a common mechanism. J. Biol. Chem. 282 (10), 7576–7581. https://doi.org/10.1074/jbc.M608618200. Epub 20070104PubMed PMID: 17204473.
Ouyang, W., Cen, M., Yang, L., Zhang, W., Xia, J., Xu, F., 2021. NMI facilitates influenza A virus infection by promoting degradation of IRF7 through TRIM21. Am. J. Respir. Cell Mol. Biol. 65 (1), 30–40. https://doi.org/10.1165/rcmb.2020-0391OC. PubMed PMID: 33761305.
Palomino-Segura, M., Perez, L., Farsakoglu, Y., Virgilio, T., Latino, I., D'Antuono, R., et al., 2019. Protection against influenza infection requires early recognition by inflammatory dendritic cells through C-type lectin receptor SIGN-R1. Nat. Microbiol. 4 (11), 1930–1940. https://doi.org/10.1038/s41564-019-0506-6. Epub 20190729PubMed PMID: 31358982; PubMed Central PMCID: PMCPMC6817362.
Perales-Linares, R., Navas-Martin, S., 2013. Toll-like receptor 3 in viral pathogenesis: friend or foe? Immunology 140 (2), 153–167. https://doi.org/10.1111/imm.12143. PubMed PMID: 23909285; PubMed Central PMCID: PMCPMC3784162.
R_Core_Team, 2013a. R: A Language and Environment for Statistical Computing. R Foundation for Statistical Computing, Vienna, Austria. http://www.R-project.org/.
Salomon, R., Hoffmann, E., Webster, R.G., 2007. Inhibition of the cytokine response does not protect against lethal H5N1 influenza infection. Proc. Natl. Acad. Sci. U.S.A 104 (30), 12479–12481. https://doi.org/10.1073/pnas.0705289104. Epub 20070717PubMed PMID: 17640882; PubMed Central PMCID: PMCPMC1924467.
Seo, S.H., Webster, R.G., 2002. Tumor necrosis factor alpha exerts powerful anti-influenza virus effects in lung epithelial cells. J. Virol. 76 (3), 1071–1076. https://doi.org/10.1128/jvi.76.3.1071-1076.2002. PubMed PMID: 11773383; PubMed Central PMCID: PMCPMC135862.
Shen, Y., Li, N.L., Wang, J., Liu, B., Lester, S., Li, K., 2012. TRIM56 is an essential component of the TLR3 antiviral signaling pathway. J. Biol. Chem. 287 (43),

36404–36413. https://doi.org/10.1074/jbc.M112.397075. Epub 20120904PubMed PMID: 22948160; PubMed Central PMCID: PMCPMC3476306.
Smith, C.L., Blake, J.A., Kadin, J.A., Richardson, J.E., Bult, C.J., 2018. Mouse genome database G. Mouse genome database (MGD)-2018: knowledgebase for the laboratory mouse. Nucleic. Acids. Res. 46 (D1), D836–DD42. https://doi.org/10.1093/nar/gkx1006. PubMed PMID: 29092072; PubMed Central PMCID: PMCPMC5753350.
Smith, J.R., Hayman, G.T., Wang, S.J., Laulederkind, S.J.F., Hoffman, M.J., Kaldunski, M.L., et al., 2020. The year of the rat: the rat genome database at 20: a multi-species knowledgebase and analysis platform. Nucleic. Acids. Res. 48 (D1), D731–DD42. https://doi.org/10.1093/nar/gkz1041. PubMed PMID: 31713623; PubMed Central PMCID: PMCPMC7145519.
Snelgrove, R.J., Edwards, L., Rae, A.J., Hussell, T, 2006. An absence of reactive oxygen species improves the resolution of lung influenza infection. Eur. J. Immunol. 36 (6), 1364–1373. https://doi.org/10.1002/eji.200635977. PubMed PMID: 16703568.
Solorzano, A., Webby, R.J., Lager, K.M., Janke, B.H., Garcia-Sastre, A., Richt, J.A., 2005. Mutations in the NS1 protein of swine influenza virus impair anti-interferon activity and confer attenuation in pigs. J. Virol. 79 (12), 7535–7543. https://doi.org/10.1128/JVI.79.12.7535-7543.2005. PubMed PMID: 15919908; PubMed Central PMCID: PMCPMC1143661.
Sparrer, K.M.J., Gableske, S., Zurenski, M.A., Parker, Z.M., Full, F., Baumgart, G.J., et al., 2017. TRIM23 mediates virus-induced autophagy via activation of TBK1. Nat. Microbiol. 2 (11), 1543–1557. https://doi.org/10.1038/s41564-017-0017-2. Epub 20170904PubMed PMID: 28871090; PubMed Central PMCID: PMCPMC5658249.
Srivastava, B., Blazejewska, P., Hessmann, M., Bruder, D., Geffers, R., Mauel, S., et al., 2009. Host genetic background strongly influences the response to influenza a virus infections. PLoS ONE 4 (3), e4857. https://doi.org/10.1371/journal.pone.0004857. Epub 20090318PubMed PMID: 19293935; PubMed Central PMCID: PMCPMC2654507.
Stacey, K.B., Breen, E., Jefferies, C.A., 2012. Tyrosine phosphorylation of the E3 ubiquitin ligase TRIM21 positively regulates interaction with IRF3 and hence TRIM21 activity. PLoS ONE 7 (3), e34041. https://doi.org/10.1371/journal.pone.0034041. Epub 20120330PubMed PMID: 22479513; PubMed Central PMCID: PMCPMC3316593.
Strandberg, L., Ambrosi, A., Espinosa, A., Ottosson, L., Eloranta, M.L., Zhou, W., et al., 2008. Interferon-alpha induces up-regulation and nuclear translocation of the Ro52 autoantigen as detected by a panel of novel Ro52-specific monoclonal antibodies. J. Clin. Immunol. 28 (3), 220–231. https://doi.org/10.1007/s10875-007-9157-0. PubMed PMID: 18071879.
Varich, N.L., Kochergin-Nikitsky, K.S., Usachev, E.V., Usacheva, O.V., Prilipov, A.G., Webster, R.G., et al., 2009. Location of antigenic sites recognized by monoclonal antibodies in the influenza A virus nucleoprotein molecule. J. Gen. Virol. 90 (Pt 7), 1730–1733. https://doi.org/10.1099/vir.0.010660-0. Epub 20090318PubMed PMID: 19297605; PubMed Central PMCID: PMCPMC2889452.
Wang, J.P., Bowen, G.N., Padden, C., Cerny, A., Finberg, R.W., Newburger, P.E., et al., 2008. Toll-like receptor-mediated activation of neutrophils by influenza A virus. Blood 112 (5), 2028–2034. https://doi.org/10.1182/blood-2008-01-132860. Epub 20080610PubMed PMID: 18544685; PubMed Central PMCID: PMCPMC2518904.
Wang, N., Liang, Y., Devaraj, S., Wang, J., Lemon, S.M., Li, K., 2009. Toll-like receptor 3 mediates establishment of an antiviral state against hepatitis C virus in hepatoma cells. J. Virol. 83 (19), 9824–9834. https://doi.org/10.1128/JVI.01125-09. Epub 20090722PubMed PMID: 19625408; PubMed Central PMCID: PMCPMC2747996.
Watkinson, R.E., McEwan, W.A., Tam, J.C., Vaysburd, M., James, L.C., 2015. TRIM21 promotes cGAS and RIG-I sensing of viral genomes during infection by antibody-opsonized virus. PLoS. Pathog. 11 (10), e1005253 https://doi.org/10.1371/journal.ppat.1005253. Epub 20151027PubMed PMID: 26506431; PubMed Central PMCID: PMCPMC4624778.
Watkinson, R.E., Tam, J.C., Vaysburd, M.J., James, L.C., 2013. Simultaneous neutralization and innate immune detection of a replicating virus by TRIM21. J. Virol. 87 (13), 7309–7313. https://doi.org/10.1128/JVI.00647-13. Epub 20130417PubMed PMID: 23596308; PubMed Central PMCID: PMCPMC3700317.
Weber, G.F., Chousterman, B.G., He, S., Fenn, A.M., Nairz, M., Anzai, A., et al., 2015. Interleukin-3 amplifies acute inflammation and is a potential therapeutic target in sepsis. Science 347 (6227), 1260–1265. https://doi.org/10.1126/science.aaa4268. PubMed PMID: 25766237; PubMed Central PMCID: PMCPMC4376966.
Wilk, E., Pandey, A.K., Leist, S.R., Hatesuer, B., Preusse, M., Pommerenke, C., et al., 2015. RNAseq expression analysis of resistant and susceptible mice after influenza A virus infection identifies novel genes associated with virus replication and important for host resistance to infection. BMC Genomics 16 (1), 655. https://doi.org/10.1186/s12864-015-1867-8. Epub 20150902PubMed PMID: 26329040; PubMed Central PMCID: PMCPMC4557482.
Xu, F., Gao, J., Bergmann, S., Sims, A.C., Ashbrook, D.G., Baric, R.S., et al., 2020. Genetic dissection of the regulatory mechanisms of Ace2 in the infected mouse lung. Front. Immunol. 11, 607314 https://doi.org/10.3389/fimmu.2020.607314. Epub 2021/01/26PubMed PMID: 33488611; PubMed Central PMCID: PMCPMC7819859.
Xu, F., Gao, J., Bergmann, S., Sims, A.C., Ashbrook, D.G., Baric, R.S., et al., 2021. Genetic dissection of the regulatory mechanisms of Ace2 in the infected mouse lung. Front. Immunol. 11, 607314 https://doi.org/10.3389/fimmu.2020.607314. Epub 2021/01/26PubMed PMID: 33488611; PubMed Central PMCID: PMCPMC7819859.
Young, J.A., Sermwittayawong, D., Kim, H.J., Nandu, S., An, N., Erdjument-Bromage, H., et al., 2011. Fas-associated death domain (FADD) and the E3 ubiquitin-protein ligase TRIM21 interact to negatively regulate virus-induced interferon production. J. Biol. Chem. 286 (8), 6521–6531. https://doi.org/10.1074/jbc.M110.172288. Epub 20101223PubMed PMID: 21183682; PubMed Central PMCID: PMCPMC3057824.
Yu, G., Wang, L.G., Han, Y., He, Q.Y., 2012. clusterProfiler: an R package for comparing biological themes among gene clusters. OMICS. 16 (5), 284–287. https://doi.org/10.1089/omi.2011.0118. Epub 20120328PubMed PMID: 22455463; PubMed Central PMCID: PMCPMC3339379.
Zhao, J., Wohlford-Lenane, C., Zhao, J., Fleming, E., Lane, T.E., McCray Jr., P.B., et al., 2012. Intranasal treatment with poly(I*C) protects aged mice from lethal respiratory virus infections. J. Virol. 86 (21), 11416–11424. https://doi.org/10.1128/JVI.01410-12. Epub 20120822PubMed PMID: 22915814; PubMed Central PMCID: PMCPMC3486278.
Zhou, Z., Jiang, X., Liu, D., Fan, Z., Hu, X., Yan, J., et al., 2009. Autophagy is involved in influenza A virus replication. Autophagy 5 (3), 321–328. https://doi.org/10.4161/auto.5.3.7406. Epub 20090414PubMed PMID: 19066474.